Journal of Catalysis 278 (2011) 26–40

Contents lists available at ScienceDirect

Journal of Catalysis

journal homepage: www.elsevier.com/locate/jcat

Correlating the preparation and performance of cobalt catalysts supported on carbon nanotubes and carbon spheres in the Fischer–Tropsch synthesis

Haifeng Xiong [a,b], Myriam A.M. Motchelaho [b,c], Mahluli Moyo [b,c], Linda L. Jewell [c], Neil J. Coville [a,b,*]

[a] DST/NRF Centre of Excellence in Strong Materials, University of the Witwatersrand, Johannesburg 2050, South Africa
[b] Molecular Sciences Institute, School of Chemistry, University of the Witwatersrand, Johannesburg 2050, South Africa
[c] School of Chemical and Metallurgical Engineering, University of the Witwatersrand, Johannesburg 2050, South Africa

ARTICLE INFO

Article history:
Received 8 September 2010
Revised 26 October 2010
Accepted 13 November 2010
Available online 28 December 2010

Keywords:
Fischer–Tropsch synthesis
Cobalt catalysts
Carbon nanotubes
Carbon spheres
Autoreduction
Particle size
Turnover frequency
Selectivity

ABSTRACT

A series of Co catalysts supported on carbon nanotubes (CNTs) and carbon spheres (CSs) with different cobalt particle sizes (3–45 nm) were prepared by different methods and using different cobalt precursors. The Co/CNTs and Co/CSs can be autoreduced by the supports in N_2 at ca. 480 °C; they show better Fischer–Tropsch performance than those reduced in H_2 when the reduction $T > 400$ °C. The turnover frequency (TOF) value for both Co/CNT and Co/CS was constant for cobalt particles above 10 nm and decreased sharply for the cobalt catalysts with smaller cobalt particles. Remarkably, the TOF for 11 catalysts prepared using different precursors and preparation methods on two different carbon supports depends only on particle size. Finally, a positive relationship was observed between cobalt particle size and C_{5+} selectivity for both Co/CNT and Co/CS catalysts.

1. Introduction

Fischer–Tropsch synthesis (FTS) is known as a reaction that produces hydrocarbons from syngas (CO and H_2) derived from coal, natural gas, or biomass and is used for making chemicals and transportation fuels [1–5]. The FTS catalyst is typically placed on a support, and the supports used include Al_2O_3, SiO_2, TiO_2, and MgO. However, the use of these supports can generate a strong metal–support interaction with the classical FT catalysts, Fe and Co. This can even lead to the formation of mixed compounds such as Co_2SiO_2 [6,7], Co_2AlO_4 [8,9], or $CoTiO_4$ [10], which are reducible only at high reduction temperatures. To lower this interaction, some costly metals such as Ru, Pt, and Re can be added to the Co to assist with the reduction of the cobalt oxides. An alternative is to use carbon as the support instead of a metal oxide. The use of inert carbon materials as supports for cobalt FTS catalysts is an effective method to enhance the reducibility of cobalt oxide. Indeed, carbon has been shown to have further benefits over metal oxides as supports. These include cost, easy removal of supports by oxidation to recover precious metals, limited micro-porosity, etc. Recently, great attention has been paid to catalysts supported on novel carbon nanostructured materials such as carbon nanofibers (CNFs) [11,12], multi-walled carbon nanotubes (MWCNTs) [13], and carbon spheres (CSs) [14] for use in the FT reaction. De Jong and coworkers have used fish-bone-like CNFs as a model support to systematically study cobalt FTS catalysts [11,12]. They found that the turnover frequency (TOF) for CO hydrogenation was independent of cobalt particle size for catalysts with sizes larger than 6–8 nm [11]. The lower TOF of catalysts for smaller cobalt particles was caused by both blocking of edge/corner sites and a lower intrinsic activity at the small terraces.

MWCNTs represent an interesting alternative to conventional supports for reasons that include their impressive mechanical properties, the high accessibility of the active phase, and the absence of any micro-porosity, thus eliminating intraparticle mass transfer in the reaction medium. Further, their specific surface area can be modulated between 50 and 500 $m^2\,g^{-1}$, and their internal diameter can be adjusted from 5 to 100 nm [15]. MWCNT-based catalysts have been used for the Fischer–Tropsch reaction. A Fe/MWCNT catalyst has been found to be a very stable and active FTS catalyst [16]. Guczi et al. [17] reported that high catalytic activity and high selectivity toward C_{5+} fractions were obtained from Fe/CNT catalysts prepared by impregnation methods. Kang et al. [13] reported that Ru nanoparticles supported on carbon nanotubes, with a mean size around 7 nm, exhibited the highest

---

* Corresponding author at: DST/NRF Centre of Excellence in Strong Materials, University of the Witwatersrand, Johannesburg 2050, South Africa. Fax: +27 11 717 6749.

E-mail address: Neil.Coville@wits.ac.za (N.J. Coville).

0021-9517/$ - see front matter © 2010 Elsevier Inc. All rights reserved.
doi:10.1016/j.jcat.2010.11.010

C_{10}–C_{20} selectivity (ca. 65%) and a relatively higher TOF for CO conversion. Recently, it has been found that MWCNT-encapsulated iron catalysts showed higher FTS activity than catalysts with iron nanoparticles dispersed on the outer walls of MWCNTs [3,18]. CNT-supported cobalt-based catalysts with different loadings of cobalt, ruthenium, and potassium have also been studied in the Fischer–Tropsch synthesis [19]. It has been found that for a 15 wt.%Co/CNT catalyst, most of the metal nanoparticles were homogeneously dispersed in the internal cavity of the MWCNTs, but increasing the cobalt loading to 30 wt.% increased the amount of cobalt on the outer surface of the CNTs. This resulted in an increase in the cobalt particle size and a decrease in the reduction temperature and dispersion. More recently, Zhang et al. [20] showed that the use of carbon nanotubes with different outer diameters did not affect cobalt dispersion and that carbon nanotubes with different diameters exhibited similar cobalt particle sizes with similar reducibility. It appears that cobalt particle size in cobalt catalysts supported on CNTs is mostly influenced by chemical interactions between the cobalt and the nanotubes, which probably occur during decomposition of the cobalt precursor, and nucleation and growth of cobalt oxide crystallites.

Carbon spheres (CSs) are composed of random curling graphitic flakes with a size of 1–10 nm and are similar to CNTs, in having carbon atoms with sp^2 hybridization [21,22]. The CSs are expected to have analogous chemical characteristics to CNTs. When prepared by chemical vapor deposition, the carbon spheres are formed without a catalyst and no purification is needed. Furthermore, they are non-porous and can be expected to be good model supports in catalysis [23]. Carbon spheres have been known for decades, but recent studies have led to added information on their synthesis, chemistry, and properties. Recent preliminary studies on Co/CS catalysts showed that the cobalt oxide can be autoreduced by the carbon spheres and that the autoreduced catalyst shows better FTS performance in comparison with a catalyst reduced in H_2 [14]. More significantly, it was observed that the Co particles could readily be detected by electron microscopy techniques. Model iron FTS catalysts supported on carbon spheres have also been prepared to investigate the effect of the preparation method, iron precursor, and promoters on FTS performance [23]. A good match of results with previous studies on non-carbon supports has been obtained. Recently, nickel catalysts supported on carbon spheres have been investigated in the hydrogenation of butyronitrile [24,25].

Although CNTs are often shown to have a smooth outer wall consisting of a single graphene layer (in structural diagrams of models used for computational chemistry), TEM studies seldom give evidence of these ‘ideal’ surfaces, especially images of MWCNTs. Rather, the CNT surface is covered with flake-like aggregates [26], similar to the surface of a CS. To illustrate this, a cartoon of a typical CNT and a CS is shown in Fig. 1. Given the similarity in their surfaces, one would expect CNTs and CSs to behave in a similar way when used as catalyst supports. Yet, in work reported to date, no comparative study between the effect of CNTs and CSs has been undertaken.

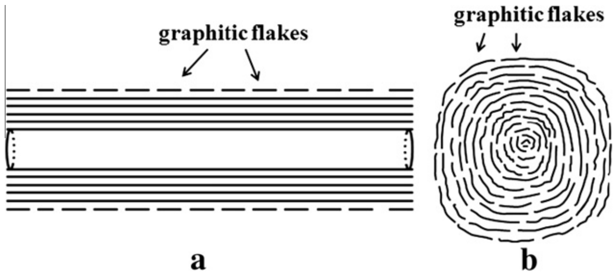

Fig. 1. Cartoon of (a) a carbon nanotube and (b) a carbon sphere.

In this study, similarities and differences between Co/CNT and Co/CS catalysts have been investigated. The autoreduction and the effect of precursor and preparation methods of the catalysts on FTS performance are investigated. Carbon nanotubes and carbon spheres were prepared by a chemical vapor deposition method. Cobalt FTS catalysts supported on carbon nanotubes and carbon spheres were made by different methods (impregnation and deposition precipitation) and using different cobalt precursors (cobalt nitrate and cobalt acetate). These catalysts were characterized by a range of techniques, and their FT activity was evaluated in a fixed-bed reactor.

2. Experimental

2.1. Sample preparation

2.1.1. The preparation of MWCNTs and CSs

A 5%Co/5%Fe/$CaCO_3$ catalyst was prepared by wet impregnation of a $CaCO_3$ support with an aqueous cobalt nitrate and an iron nitrate solution as described in our previous study [27]. In a previous publication [27], we performed a systematic study of the synthesis of CNTs using Fe and Co on $CaCO_3$. In that study, the conditions (temperature, flow rates, gas mixtures, and catalyst composition) to produce very pure CNTs were established. These conditions were used in this study. The advantage of the support used is that the $CaCO_3$ is easy to remove with dilute acid. Briefly, calculated amounts of the Fe and Co nitrates were mixed and dissolved in distilled water, and then, the resulting solution was impregnated directly onto the $CaCO_3$ support. Subsequently, the material was aged for 12 h in air at room temperature, followed by drying at 120 °C for 12 h and calcining in air at 600 °C for 17 h. A tubular quartz reactor (510 mm × 19 mm i.d.) was placed horizontally in a furnace and was used to pyrolyze acetylene and synthesize carbon nanotubes by the catalytic chemical vapor deposition method using the as-prepared 5%Co/5%Fe/$CaCO_3$ as catalyst.

The detailed experimental procedures are as follows: the catalyst (0.5 g) was spread to form a thin layer in a quartz boat (120 mm × 15 mm), and the boat was then placed in the center of the quartz tube. The furnace was then heated at 10 °C min^{-1} under flowing N_2 (40 mL min^{-1}). Once the temperature had reached 700 °C, the N_2 flow rate was set to 240 mL min^{-1} and C_2H_2 was introduced at a constant flow rate of 90 mL min^{-1}. After 60 min of reaction time, the C_2H_2 flow was stopped and the furnace was left to cool down to room temperature under a continuous flow of N_2 (40 mL min^{-1}). The boat was then removed from the reactor, and the carbon deposit that formed on the surface of the catalyst was collected.

Carbon spheres (CSs) were prepared by a chemical vapor deposition method [23]. A tubular quartz reactor was placed horizontally in a furnace. The acetylene was pyrolyzed in the tube and generated the carbon spheres. The temperature in the reactor was firstly increased to 900 °C in a flow of N_2 (40 mL min^{-1}). Subsequently, acetylene was introduced into the reactor at a flow rate of 100 mL min^{-1} and held at 900 °C for 1 h. The pyrolysis reaction generated a sooty deposit on the inner wall of the quartz tube in the hot region of the reactor. Finally, the reactor was cooled down to room temperature in flowing N_2, and the soot was collected, weighed, and analyzed. Scanning electron microscopy (SEM) analysis revealed that the size of the prepared carbon spheres was around 900 ± 50 nm with a BET surface area of <5 $m^2\ g^{-1}$.

2.1.2. The purification and functionalization of carbon nanotubes and carbon spheres

The purification and functionalization of CNTs were achieved using 55 vol.% HNO_3 solution. Briefly, the raw (i.e., unpurified) carbon nanotubes (1.0 g) were mixed with 55 vol.% HNO_3 (100 mL) and refluxed at 120 °C for 17 h. Then, the mixture was filtered and washed with deionized water until the pH of the mother liquor reached a value of 7. The resulting material was dried overnight at 90 °C in an oven.

For the functionalization of CSs, about 1.0 g of CSs was functionalized in 100 mL of 55 vol.% HNO_3 at different temperatures (45, 70, and 90 °C) for 17 h. Then, the mixture was filtered and washed with deionized water until the pH of the mother liquor reached a value of 7. The resulting material was dried overnight at 100 °C in an oven and denoted as CS-A, CS-B, and CS-C for CSs prepared at 45, 70, and 90 °C, respectively.

2.1.3. Catalyst preparation

Impregnation and homogeneous deposition precipitation methods were employed to prepare cobalt catalysts supported on carbon nanotubes and carbon spheres. For the impregnation method, the appropriate cobalt nitrate solution (15 wt.%) was impregnated onto the functionalized carbon nanotubes directly and then dried at 100 °C for 10 h. The catalysts prepared by impregnation were denoted as Co/CNT-IM (IM stands for impregnation). For the Co/CNT catalyst prepared by the homogeneous deposition precipitation method, urea was used as the precipitating agent and the detailed synthesis route was as follows: $Co(NO_3)_2{\cdot}6H_2O$ (0.41 g) and urea (0.27 g; 2 mol urea per mole of cobalt) were dissolved in deionized water (200 mL) and added to 0.5 g of the functionalized carbon nanotubes. Subsequently, the temperature was raised to 90 °C. After allowing sufficient time (17 h) for the hydrolysis of the urea, the sample was filtered and washed with deionized water, followed by drying at 100 °C for 10 h. The sample was denoted as Co/CNT-DP (DP stands for deposition precipitation). A Co/CNT catalyst was also prepared using cobalt acetate ($Co(OOCCH_3)_2$) as the cobalt precursor. The sample was denoted as the CoA/CNT-IM.

For the Co/CS catalysts prepared by impregnation, the appropriate cobalt precursor solution (5 wt.%) was added to the functionalized carbon spheres directly. The material was then dried at 100 °C for 10 h. The catalysts prepared by impregnation were denoted as Co/CS-N-IM (where N = A, B, and C corresponds to the functionalization temperatures of 45, 70, or 90 °C; IM refers to impregnation). For the Co catalyst prepared by the homogeneous deposition precipitation method, urea was used as the precipitating agent and the detailed synthesis route was as follows: $Co(NO_3)_2{\cdot}6H_2O$ (0.41 g) and urea (0.18 g) in a cobalt/urea ratio of 1:2 were dissolved in deionized water (200 mL) and added to 0.5 g of the functionalized carbon spheres (CS-A, CS-B, and CS-C). Subsequently, the temperature was raised to 90 °C. After allowing sufficient time (17 h) for the hydrolysis of the urea, the sample was filtered and dried at 100 °C for 10 h. The sample was denoted as Co/CS-N-DP (where N = A, B, and C corresponds to the functionalization temperatures of 45, 70, or 90 °C). A 5%Co/CS catalyst was also prepared by impregnation of acid functionalized CSs (CS-C) using cobalt acetate ($Co(OOCCH_3)_2$) as the cobalt precursor. The preparation procedure for the catalyst was the same as that used to make 5Co/CS-C-IM. The obtained sample was denoted as CoA/CS-C-IM.

It should be mentioned that a portion of the obtained cobalt catalyst prepared above was saved for TEM characterization as well as for FTS study. Another portion of the supported cobalt catalyst was calcined in a flow of N_2 at 250 °C for 4 h for XRD and N_2 adsorption desorption measurements.

2.2. Catalyst characterization

2.2.1. X-ray powder diffraction (XRD)

X-ray powder diffraction spectra for the calcined catalysts were recorded with a Siemens D5 using Cu Kα radiation and a Ni filter. The scan range was 15°–90° with 0.002° steps. A Bruker D8 powder X-ray diffractometer with monochromatic Cu Kα radiation and Ni filter equipped with a VANTEC-1 detector was used for the in situ XRD measurements. A reactor cell (Anton Paar) mounted on a goniometer was used for in situ measurement under different atmospheres. Prior to the XRD measurement, the reactor was flushed with high-purity argon at 150 °C for 1 h, to drive off the water and other impurities, and then cooled down to 100 °C. The diffractograms were recorded from 15° to 90° with 0.016° steps. Crystallite phases were determined by comparing the diffraction patterns with those in the standard powder XRD files (JCPDS) published by the International Center for Diffraction Data.

2.2.2. N_2 adsorption–desorption

N_2 adsorption–desorption experiments were conducted at −193 °C using a Micromeretics Tristar 3000 surface area and porosity analyzer. Prior to an experiment, the sample was outgassed at 200 °C for 6 h. The BET surface areas were obtained for adsorption data in a relative pressure range from 0.05 to 0.30. The total pore volumes were calculated from the amount of N_2 vapor adsorbed at a relative pressure of 0.99. The pore size distributions were evaluated from the desorption branches of the isotherms using the Barrett–Joyner–Halenda (BJH) method.

2.2.3. Thermogravimetric analysis (TGA)

Thermogravimetric analysis was performed with a Perkin-Elmer STA6000 TGA using nitrogen or air as the purge gas and a heating rate of the 10 °C min^{-1}. The flow rate of the purge gas was always 20 mL min^{-1}.

2.2.4. Transmission electron microscopy (TEM)

TEM analysis was performed on a Tecnai spirit transmission electron microscope at 120 kV, and high-resolution transmission electron microscopy was carried out on a FEI Tecnai F20 FEGTEM at 200 kV. An ex situ reduction step (under H_2 or Ar atmosphere) was used to reduce and passivate the catalysts. The pre-reduction and passivation were carried out in a fixed-bed reactor. Firstly, the sample was reduced at different temperatures (300, 400, and 480 °C) for 20 h. Subsequently, the temperature was decreased to 30 °C, and then, 1% O_2/He (30 mL min^{-1}) was introduced into this system to passivate the sample for 6 h. After these steps, the passivated catalyst was dispersed in methanol using a sonicator and loaded onto a copper grid. The particle size of the cobalt formed was determined by counting at least 100 'shaped objects' per sample. These were randomly chosen from different TEM images. Common Gaussian statistics yields values for the average cobalt diameter.

2.2.5. Temperature-programmed reduction (TPR)

The TPR experiment was carried out with a Micromeritics Auto Chem II unit. The catalyst (ca. 0.1 g) was placed in a quartz tubular reactor, fitted with a thermocouple for continuous temperature measurement. The reactor was heated with a furnace. Prior to the temperature-programmed reduction measurement, the calcined catalysts were flushed with high-purity argon at 150 °C for 1 h, to drive away the water or impurities, and then cooled down to 50 °C. Then, 5% H_2/Ar was switched on, and the temperature was raised at a rate of 10 °C min^{-1} from 50 to 800 °C (hold 10 min). The gas flow rate through the reactor was controlled by three Brooks mass flow controllers and was always 50 cm^3 min^{-1}. The H_2 consumption (TCD signal) was recorded automatically by a PC.

2.2.6. H_2 Chemisorption

Hydrogen chemisorption was carried out in a U-tube quartz reactor with a Micromeritics ASAP 2020 unit to give the number of active surface metal atoms. The sample weight used was ca. 0.200 g. The catalyst was first evacuated to 10^{-6} mm Hg at 100 °C for 1 h. The catalyst was then reduced at 400 °C for 16 h using a flow of high-purity hydrogen and evacuated at 400 °C for 1 h to desorb any H_2. Subsequently, H_2 was introduced to the system, and the chemisorption was performed at 30 °C.

2.3. Catalytic evaluation

The Fischer–Tropsch synthesis was performed in a fixed-bed micro-reactor. Gas cylinders containing $H_2/CO/N_2$ mixtures (60/30/10 vol.% purity: 99.99) were used to supply the reactant gas stream to the catalyst with a space velocity of 3840 h^{-1}. N_2 was used as an internal standard in order to ensure accurate mass balances. Catalyst (0.1 g) was added to the reactor and reduced in situ at 400 °C for 20 h under a stream of H_2 (2 bar, 30 mL min^{-1}). After reduction, the temperature was decreased to 225 °C, synthesis gas was introduced, and the pressure was increased gradually to 8 bar. All gas lines after the reactor were kept at 150 °C, and a hot trap placed immediately after the reactor was held at this temperature in order to collect wax. A second trap kept at ambient temperature was used to collect the oil and water mixture. The flow was controlled using a metering valve and measured by a bubble meter. The product stream was analyzed online using two gas chromatographs. A thermal conductivity detector (TCD), equipped with a Porapak Q (1.50 m × 3 mm) packed column, was used to analyze N_2, CO, and CO_2, and a flame ionization detector (FID), equipped with a Porapak Q packed column, was used for the analysis of hydrocarbons.

3. Results and discussion

3.1. Support and cobalt catalyst characterization

3.1.1. Carbon nanotubes and Co/CNT catalysts

The XRD patterns of some of the prepared Co/CNT catalysts thermally treated in N_2 are displayed in Fig. 2. For both Co/CNT-IM and CoA/CNT-IM, the XRD patterns (Fig. 2a and b) show diffraction peaks at 31.5°, 37.0°, 44.9°, 59.6°, and 65.5°, corresponding to the different crystal planes of the Co_3O_4 phase, as well as a relatively sharp peak (β) between 20° and 30° due to the carbon (Fig. S1). No XRD pattern for Co_3O_4 was observed for Co/CNT-DP (Fig. 2c). This is probably because the cobalt particles on this catalyst are too small to be detected by XRD (<4 nm) [28], as revealed by TEM images (see below).

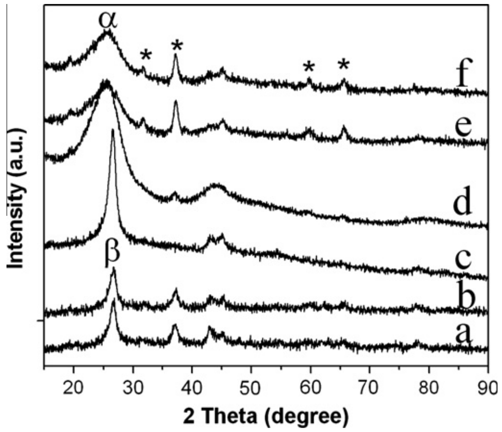

Fig. 2. XRD patterns of calcined Co/CNT and Co/CS catalysts: (a) Co/CNT-IM; (b) CoA/CNT-IM; (c) Co/CNT-DP; (d) Co/CS-C-DP; (e) Co/CS-C-IM; (f) CoA/CS-C-IM, α: CSs; β: CNTs; ∗: Co_3O_4.

Table 1
N_2 adsorption–desorption data of the carbon supports and cobalt catalysts.

Sample	BET surface area[a] (m^2/g)	Total pore volume (cm^3/g)	Average pore size (nm)
Raw CNTs	46.4	0.18	16.1
CNTs	79.1	0.30	14.9
Co/CNT-IM	73.4	0.28	15.2
CoA/CNT-IM	103.9	0.36	13.6
Co/CNT-DP	91.7	0.39	17.3
CS-A	1.5	0.0025	–
CS-B	1.6	0.0033	–
CS-C	2.6	0.0046	–
Co/CS-C-IM	2.5	0.0095	–
CoA/CS-C-IM	2.4	0.0093	–
Co/CS-A-DP	2.3	0.0048	–
Co/CS-B-DP	3.0	0.0063	–
Co/CS-C-DP	3.4	0.0094	–

[a] The uncertainties in the BET surface area <5 m^2/g (for density <1 g/cm^3) are large.

BET surface areas and pore volumes of the functionalized carbon nanotubes and cobalt catalysts are displayed in Table 1. As can be seen, a relatively low pore volume and BET surface area for raw CNTs are observed. After the raw CNTs were purified with HNO_3, the BET surface area and total pore volume increased. This indicated that the treatment of the raw CNTs in nitric acid at 120 °C for 17 h has removed the residual Fe–Co/CaO. Compared to the respective supports, the cobalt-loaded catalysts showed significantly higher BET surface area and pore volume.

Fig. 3 displays the TGA/DTG curves of the unpurified CNTs, the purified CNTs, and the Co/CNT catalysts prepared under both air and N_2 atmospheres. The peak position of weight loss is given in Table S1. For unpurified carbon nanotubes, the sample is stable below 500 °C and a ca. 80% weight loss can be detected when the pristine CNTs are heated to 900 °C under air (Fig. 3a) due to the loss of the carbon by oxidation. The residual weight is attributed to the Fe-Co/CaO catalyst used during the preparation of CNTs. The relative DTG curve shows two distinct weight loss peaks between 500 and 750 °C (Table S1). After the raw CNTs were refluxed in 55% HNO_3 for 17 h, the TGA curve of the purified CNTs shows that the sample is entirely oxidized at 700 °C under air (Fig. 3b). The relative DTG curve indicated that three weight loss peaks exist, located at 60 °C, 150–350 °C, and 650 °C, respectively. TGA experiments in a nitrogen atmosphere were performed to assess the thermal stability of the samples. The TGA/DTG curves of purified CNTs under N_2 are shown in Fig. 3c. It can be seen that a ca. 20% weight loss can be detected when the sample is heated to 900 °C. Three weight loss peaks at 60 °C, 250 °C, and 700 °C were found in the DTG curve.

Generally, a weight loss below 100 °C is considered to be due to the release of absorbed water in the sample. A weight loss between 150 and 350 °C for the purified CNTs is attributed to the removal of functional groups (–COOH and –OH) chemically bonded on the carbon nanotube surface. The weight loss observed for CNTs above 500 °C is ascribed to the loss of the non-graphitic carbon. These TGA data under N_2 show that the carbon nanotubes pretreated in nitric acid contain functionalized groups [3,23].

For the uncalcined Co/CNT-IM catalyst using cobalt nitrate as a precursor, TGA data under N_2 (Fig. 3d) reveal that four major weight loss events take place at 50–150 °C, 200–400 °C, and 500–600 °C. The first weight loss (50–150 °C) is attributed to the removal of water, and the two weight loss peaks between 200 and 400 °C are attributed to the nitrate group decomposition of the cobalt nitrate precursor. The fourth one (500–600 °C) is attributed to the loss of non-graphitic carbon. The TGA curve of the uncalcined cobalt catalyst prepared from $Co(OOCCH_3)_2$ is shown in Fig. 3e. As can be seen, there are two weight loss peaks between 50 and

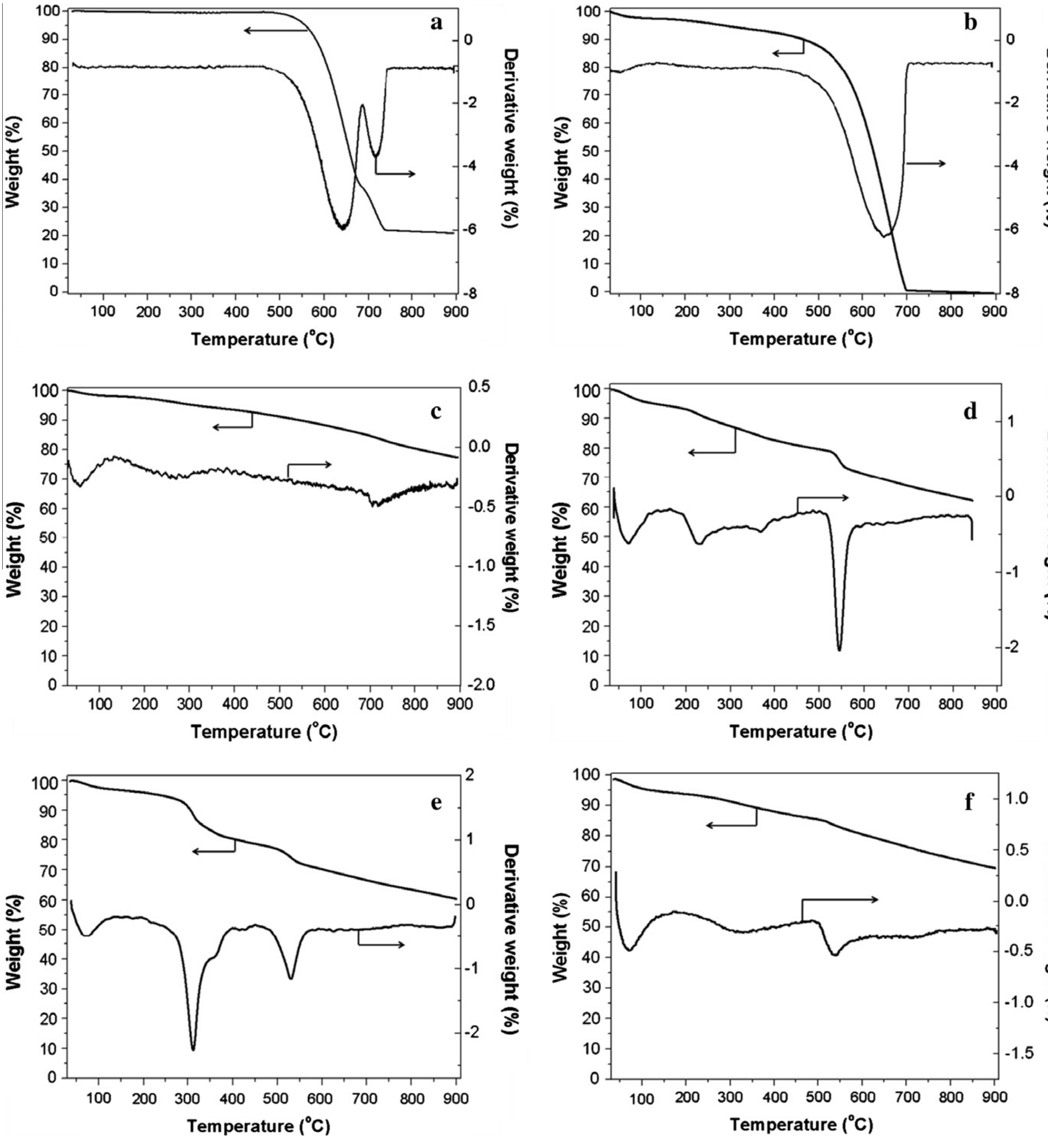

Fig. 3. TGA curves of pristine and functionalized carbon nanotubes and cobalt catalysts under N_2 or air: (a) pristine CNTs under air; (b) functionalized CNTs under air; (c) functionalized CNTs under N_2; (d) uncalcined Co/CNT-IM under N_2; (e) uncalcined CoA/CNT-IM under N_2; (f) uncalcined Co/CNT-DP in N_2.

400 °C as well as a weight loss peak located at ca. 530 °C. The peaks between 50 and 400 °C can be assigned to the removal of water and the decomposition of acetate ions. The weight loss of the prepared Co/CNT-DP under N_2 is shown in Fig. 3f. Three significant weight loss peaks are found in the DTG curve, located at 70, 310, and 540 °C, respectively. Similarly, these can be attributed to the loss of water, nitrate decomposition, and the loss of non-graphitic carbon.

Typical TEM images of unpurified and purified CNTs are shown in Fig. 4. As can be seen, some particles (Fe–Co/CaO) were found to be encapsulated in the unpurified carbon nanotubes (circles in Fig. 4a). The average pore size and outer diameter of the raw carbon nanotube are ca. 9 and 29 nm, respectively. Further, it is noted that some of the tips of the raw CNTs are opened (arrows in Fig. 4b). Fig. 4c and d shows the low-resolution and high-resolution TEM images of purified CNTs, respectively. As can be seen in Fig. 4d, the high-resolution TEM image of purified CNTs reveals that a tubular graphene structure is present parallel to the pore direction and a curved graphene structure is present perpendicular to the pore direction.

TEM images were recorded after Co had been added to the prepared CNTs. The TEM images and histograms of the relative cobalt particle size of passivated Co/CNT catalyst (pretreated in H_2 or N_2) using different preparation methods and different cobalt precursors are shown in Figs. 5–9. The Co/CNT-IM catalyst was reduced in either H_2 or N_2 at different temperatures to explore the effect of pretreatment method and temperature on the Co particle size.

Typical TEM images of Co/CNT-IM reduced in H_2 at different temperatures (300, 400, and 480 °C) are shown in Fig. 5 (400 °C) and in Fig. S2 (300 and 480 °C). The pre-reduction temperature/heating rate has a significant effect on the cobalt particle size of the catalysts. The passivated Co/CNT-IM pre-reduced at 300 °C in H_2 exhibited cobalt particles with an average particle size of 6.4 nm (Fig. S2a). Increasing the pre-reduction temperature to 400 °C, the average particle size of the cobalt declined to 3.9 nm (Fig. 5). This change is due to a different temperature ramping rate. It is interesting to note that the cobalt particle size increased markedly when the Co/CNT-IM catalyst was reduced in H_2 at 480 °C. As observed in Fig. S2b, the cobalt particle sizes are >15 nm and it seems that the cobalt particles have sintered due to the high-temperature reduction in H_2.

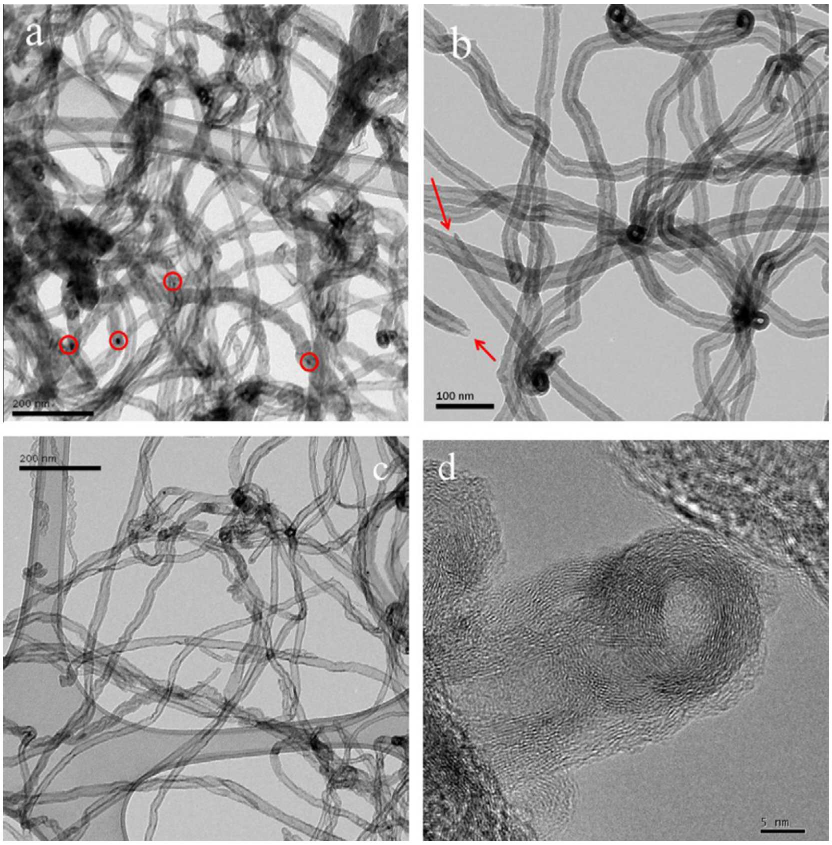

Fig. 4. Typical TEM images of carbon nanotubes: (a) showing the residual metal particle in CNTs (red circles); (b) showing some opened tips (red arrows); (c) purified carbon nanotubes; (d) high-resolution image of purified carbon nanotubes showing the structure of both the wall and edge end. (For interpretation of the references to colour in this figure legend, the reader is referred to the web version of this article.)

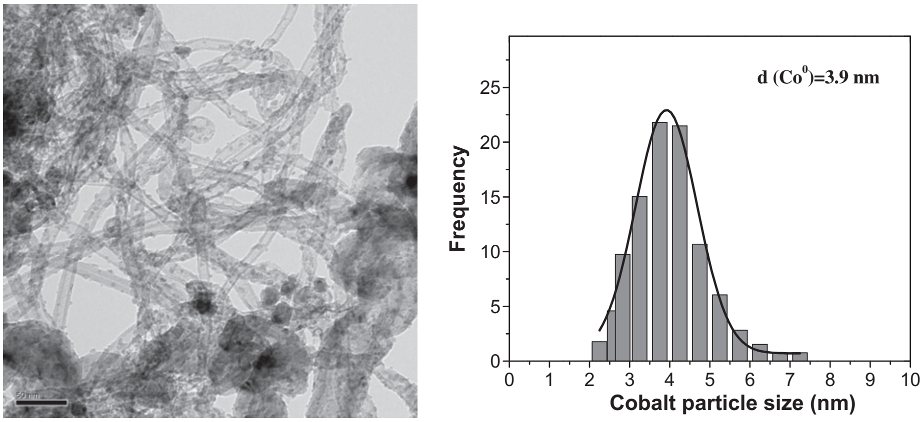

Fig. 5. Typical TEM image and cobalt particle size histogram of passivated Co/CNT-IM catalyst after reduction in H_2 at 400 °C for 20 h ($d(Co^0)$ = 3.9 nm).

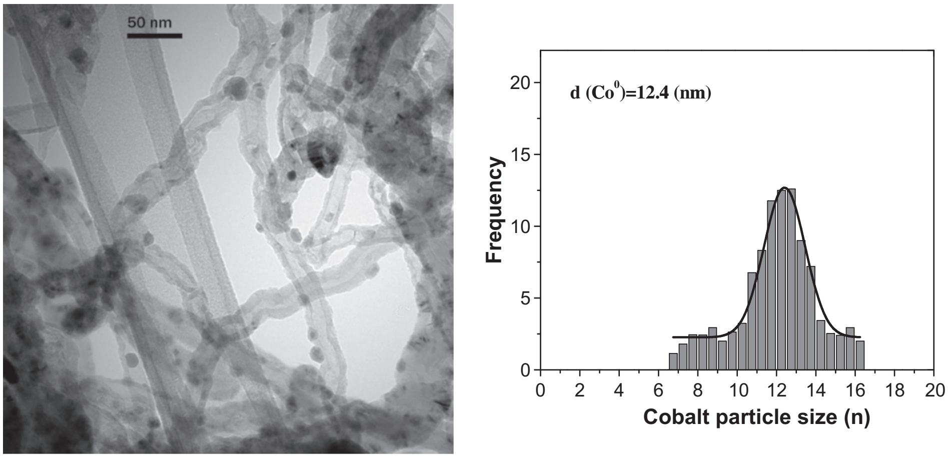

Fig. 6. Typical TEM image and cobalt particle size histogram of passivated Co/CNT-IM pretreated in N_2 at 480 °C for 20 h (d(Co^0) = 12.4 nm).

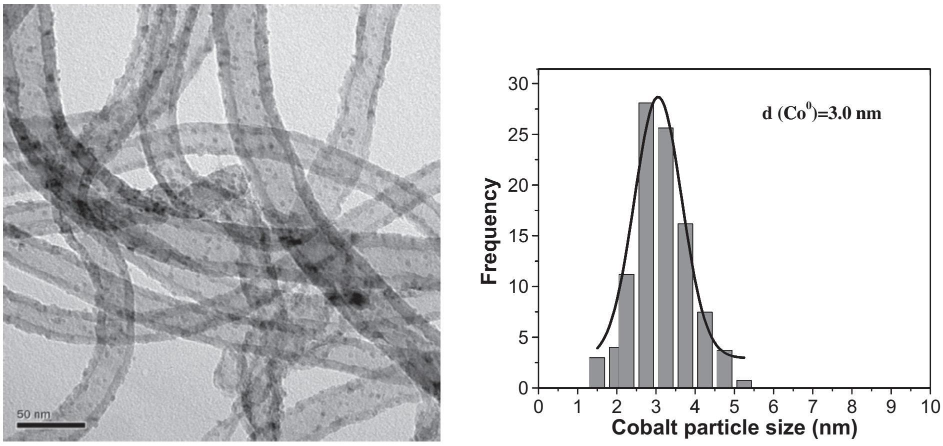

Fig. 7. Typical TEM image and cobalt particle size histogram of passivated Co/CNT-DP after reduction in H_2 at 400 °C for 20 h (d(Co^0) = 3.0 nm).

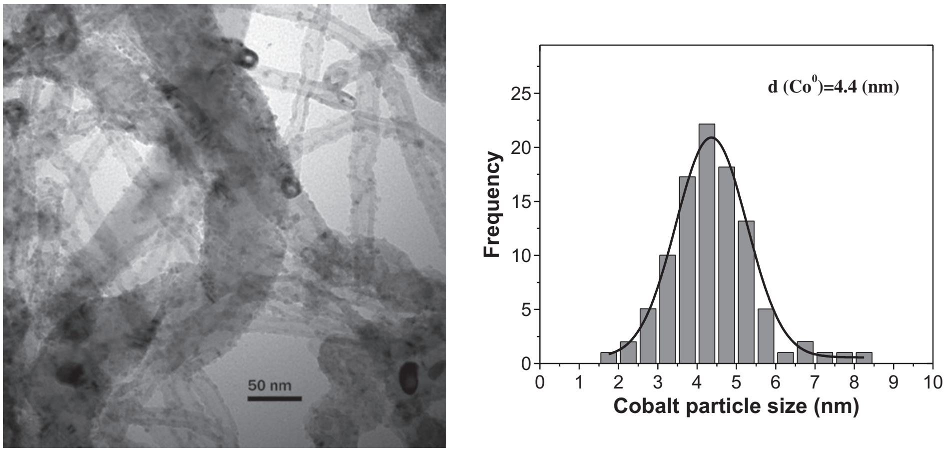

Fig. 8. Typical TEM image and cobalt particle size histogram of passivated CoA/CNT-IM after reduction in H_2 at 400 °C for 20 h (d(Co^0) = 4.4 nm).

The morphology of cobalt particles of the passivated Co/CNT-IM pretreated in N_2 at different temperatures (400 and 480 °C) has also been investigated, as shown in Fig. S3 and Fig. 6. From Fig. S3, only a small number of cobalt particles could be detected on the CNTs and this suggested that not all the cobalt oxide has been completely reduced by the carbon. When the Co/CNT-IM was pretreated in N_2 at 480 °C for 20 h (Fig. 6), cobalt particles with an average size of 12.4 nm were present on the CNT surface.

The effect of catalyst preparation method (impregnation and deposition precipitation) on the cobalt particle size of Co/CNT was studied. A typical TEM image of the passivated Co/CNT-DP pretreated in H_2 at 400 °C is shown in Fig. 7. From the histogram, an average cobalt particle size of 3.0 nm was measured. This is slightly smaller than the cobalt particle size of 3.9 nm obtained for Co/CNT-IM prepared by impregnation. Furthermore, the particle size distribution was found to be much narrower and the Co particles smaller than the cobalt particle size (8.0 nm) of similar Co/CNF catalysts prepared by deposition precipitation studied by Bezemer et al. [29].

The effect of changing cobalt nitrate to cobalt acetate on the cobalt particle size of the Co/CNT catalyst is shown in Fig. 8. An average cobalt particle size of ca. 4.4 nm was noted for CoA/CNT-IM, which is slightly larger than the cobalt particle size of 3.9 nm obtained for Co/CNT-IM. After pretreatment of CoA/CNT-IM in 5%H_2/Ar at 450 °C, the catalyst showed cobalt particles of around 16.6 nm (Fig. 9).

From Figs. 4–8, it can be seen that the cobalt particles are dispersed on both the interior and the exterior of the purified carbon nanotubes. For the Co/CNT catalysts prepared by impregnation, the majority of the cobalt particles (>70%) were dispersed on the exterior of CNT, regardless of the precursors and pretreatment methods (Figs. 5 and 6, 8 and 9). The catalyst activity is thus predominantly associated with Co particles outside the tube. This is different from the result reported by Trépanier et al. who showed that most of cobalt particles were distributed inside the tubes for a 15 wt.% Co/CNT catalyst prepared by impregnation [18]. Thus, it is suggested that the position of cobalt particles on CNTs for Co/CNT catalysts is closely associated with the preparation method, regardless of the cobalt precursors and catalyst pretreatment methods.

3.1.2. Carbon spheres (CSs) and Co/CS catalysts

For Co/CS-C-DP, a very weak Co_3O_4 signal was detected from the XRD measurement (Fig. 2d). This is due to the small cobalt particles or a low cobalt loading for this catalyst. As revealed by XRD measurements, the main cobalt phase in both the Co/CS-C-IM and CoA/CS-C-IM catalysts thermally treated in N_2 was Co_3O_4 (Fig. 2e and f). This is similar to that of Co/CNT catalysts. The peak due to carbon (20–30°) associated with CSs is more broadened than that of the CNT sample. It is known that a carbon sphere is composed of random curling graphitic flakes with a size of 1–10 nm [23], while carbon nanotubes consist of parallel graphene sheets but are typically covered with flake-like material, unless annealed [26]. The above data revealed that the main Co phase of calcined Co/CS is Co_3O_4.

TGA/DTG data were recorded on the raw carbon spheres, functionalized carbon spheres, and cobalt catalysts under N_2 and air, and the data are shown in Fig. 10 and Table S1. When pristine CSs are heated to 900 °C under N_2, a small weight loss is exhibited at around 100 °C and finally a ca. 5% weight loss can be detected (Fig. 10a). The relative DTG curve exhibits two loss weight peaks, located at 100 and 700 °C, respectively. For carbon spheres functionalized by nitric acid (CS-B), the TGA curve under N_2 is shown in Fig. 10b. It can be seen that ca. 6% weight loss is revealed when the temperature was increased to 900 °C. The relative DTG curve shows four significant weight loss peaks, which are located at 70, 270, 400, and 700 °C, respectively.

The data can readily be rationalized according to the discussion on CNTs (above) and a previous study [23]. Generally, a weight loss below 100 °C is considered to be due to the loss of absorbed water in the sample. A weight loss between 150 and 450 °C is attributed to the removal of functional groups chemically bonded on the carbon spheres surface. The weight loss observed above 500 °C is ascribed to the loss of the non-graphitic carbon. The TGA data under N_2 (Fig. 10b) also shows that the carbon spheres pretreated in nitric acid contain functionalized groups.

For the Co/CS-C-DP catalyst, the TGA curve under N_2 revealed four weight loss peaks (Fig. 10e). Compared to the support, the weight loss peak of the non-graphitic carbon for Co/CS-C-DP shifted from 680 to 550 °C (Table S1). This is consistent with that revealed for a similar Co/CNT catalyst.

Figs. 11 and 12 show typical TEM images of pristine carbon spheres and the Co/CS catalysts. As can be seen, the carbon spheres are round and smooth with an average diameter of 900 nm. It should be mentioned that from TEM characterization (Fig. S4), no significant change takes place when the carbon spheres are functionalized using nitric acid at the different temperatures used in this study. The high-resolution image (Fig. 11b) of a carbon sphere reveals that it is composed of random curling graphitic flakes, similar to those found in CNT where they are seen to be parallel to the CNT pore. A Co/CS-C-IM catalyst were prepared by impregnation, and cobalt particles with a size of 14.2 nm was found (Fig. S5). Cobalt catalysts supported on functionalized CSs were also prepared by deposition precipitation using urea hydrolysis. Typical TEM images of the passivated Co/CS pre-reduced in H_2 are shown in Fig. 12. As revealed in a previous study [23], different functionalization methods can affect the concentration of surface groups on carbon materials. The passivated Co/CS-A-DP pre-reduced in H_2 at 400 °C shows cobalt particles with $d = 45$ nm (Fig. 12a), while the passivated Co/CS-B-DP pre-reduced in H_2 at 400 °C exhibited cobalt particles with an average particle size of 12.6 nm (Fig. 12b). The passivated Co/CS-C-DP pre-reduced in H_2 at 400 °C produced cobalt particles with $d = 3.1$ nm (Fig. 12c). Furthermore, it was found that different reduction atmospheres had different effects on the cobalt particle size (Fig. 12d). The Co/CS-C-DP pretreated in 5%H_2/Ar at 480 °C showed cobalt particles with a size of ca. 21 nm.

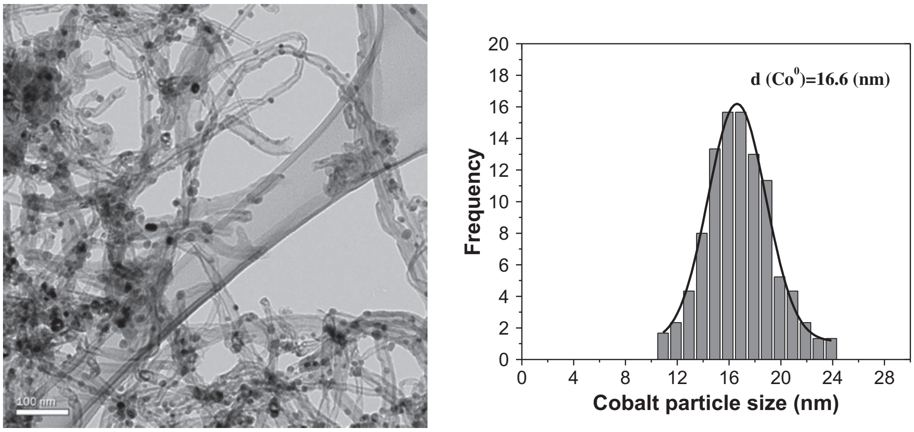

Fig. 9. Typical TEM image and cobalt particle size histogram of passivated CoA/CNT-IM reduced in 5%H_2/Ar at 450 °C for 20 h ($d(Co^0) = 16.6$ nm).

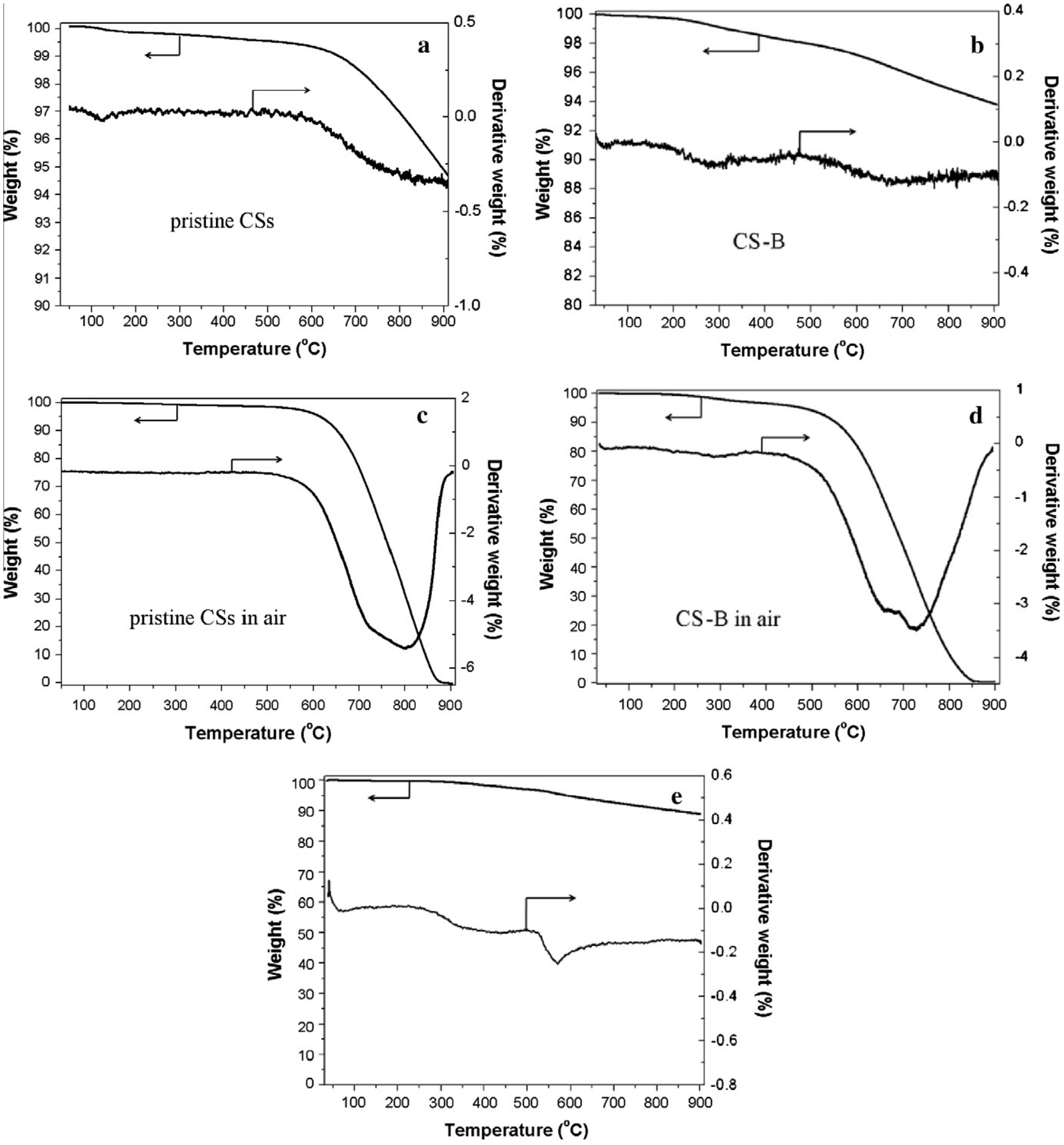

Fig. 10. TGA curves of functionalized carbon spheres and Co/CS catalysts under N_2 or air: (a) pristine CSs under N_2; (b) CS-B under N_2; (c) pristine CSs under air; (d) CS-B under air; (e) uncalcined Co/CS-C-DP in N_2.

3.1.3. Reduction of Co/CNT and Co/CS

The effect of pretreatment temperature in Ar (prior to TPR testing) on the reduction behavior of the Co/CNT-IM was monitored by H_2-TPR under 5%H_2/Ar (Fig. 13). As can be seen, the TPR profile (Fig. 13a) of Co/CNT-IM after pretreatment at 250 °C has three reduction peaks, located at 280, 363, and 477 °C, respectively. An increase in the pretreatment temperature under flowing Ar to 450 °C prior to the TPR experiment reveals the disappearance in both the first and the second reduction peaks. The third shoulder peak at 477 °C became dominant when pretreatment occurred at 450 °C for 2 h (Fig. 13b). The intensity of this third reduction peak also decreased with temperature (Fig. 13c and d). As revealed by XRD, Co_3O_4 is the main cobalt phase when Co/CNT-IM was thermally treated in N_2. Thus, the first peak at 280 °C is attributed to the reduction of Co_3O_4 to CoO, and the second reduction peak at 363 °C is attributed to the reduction of CoO to metal Co [14,30]. When compared to the TPR profile (Fig. 13e) of purified CNT support, the third reduction peak at 477 °C for the Co/CNT-IM can be attributed to the catalytic decomposition of the support. When the pretreatment temperature ⩾450 °C, no cobalt oxide phase

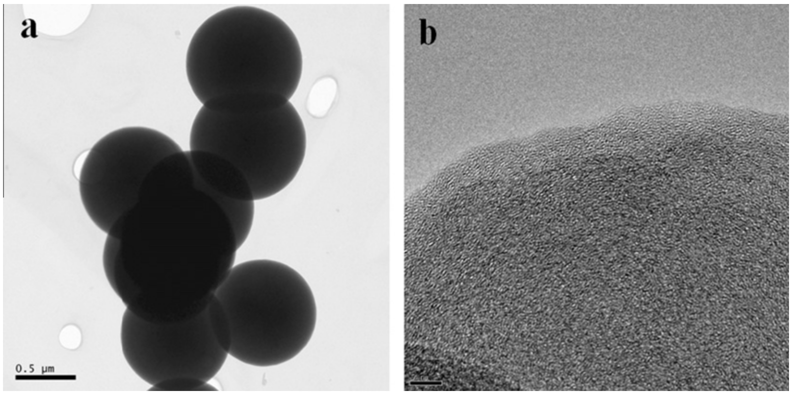

Fig. 11. TEM images of carbon spheres with (a) low resolution and (b) high resolution (scale bar: 5 nm).

was present as shown in the TPR profiles. The cobalt oxide was either reduced to Co metal or transformed to another phase which cannot be reduced in H_2 after a treatment temperature ⩾450 °C in Ar.

The phase change was also monitored by in situ X-ray diffraction. Fig. 14 shows the in situ X-ray diffraction patterns of Co/CNT-IM in an N_2 atmosphere with increasing temperature. The XRD patterns obtained in flowing N_2 revealed that the main cobalt phase observed at 30 °C is Co_3O_4. When the reduction temperature reached 400 °C, the diffraction peaks due to Co_3O_4 disappeared completely and the diffraction peaks of CoO were present, indicating that the phase transformation of Co_3O_4 to CoO was complete. It can be seen that the diffraction peaks of CoO disappeared completely when the temperature reached 480 °C, while diffraction peaks associated with cobalt metal were observed. No indication of new phases or complexes (e.g., cobalt carbides) was observed.

Based upon the above data, it is clear that cobalt oxide supported on carbon nanotubes can be reduced by the carbon support at $T \leqslant 480$ °C in an inert atmosphere to give Co that appears to be reduced under H_2. Recently, we found that cobalt oxide supported on carbon spheres could also be reduced by the carbon support at $T \leqslant 480$ °C in an inert atmosphere [14].

The π-orbital axis vector analysis shows that the chemistry of fullerene-type carbon relates directly to the strain of the graphitic network [31]. Deviation from planarity causes the partial rehybridization from sp^2 to sp^3 and the pyramidalization of the carbon atoms in curved aromatic systems. Carbon nanotubes and carbon spheres have a similar curved surface and sp^2-hybridized carbon atoms. The interaction between the convex surface of the carbon atoms and the oxygen in cobalt oxides (Co_3O_4 and CoO) could lead to weakened bonding strength within the cobalt oxides and hence lead to the reduction occurring at lower temperatures.

The TPR profiles of other Co/CNT catalysts pretreated in a flow of high-purity Ar are compared in Fig. 15. The TPR profile of a Co/CNT-DP catalyst pretreated at 250 °C for 2 h shows a reduction peak at 380 °C and a shoulder peak at 500 °C. Increasing the pretreatment temperature to 550 °C leads to the disappearance of the peak at 380 °C, i.e., the cobalt phase in the catalyst has been reduced during the pretreatment process in Ar at 550 °C.

The TPR profile of the CoA/CNT-IM catalyst also shows three reduction peaks, located at 287, 360 °C, and between 370 and 600 °C, respectively. The first peak is attributed to the reduction of Co_3O_4 to CoO. The second reduction peak is attributed to the reduction of CoO to Co^0. The intensities of both the first and the second reduction peaks are smaller, and the third reduction peak is broadened relative to those of Co/CNT-IM.

A comparison of Fig. 15a and c indicated that no Co_3O_4 is detected when the Co is generated by deposition precipitation (Co/CNT-DP).

The TPR profiles of different Co/CS catalysts pretreated in a flow of high-purity Ar are displayed in Fig. 16. The TPR profile of Co/CS-C-IM (Fig. 16a) pretreated at 120 °C for 2 h showed three distinct peaks at 150–230 °C, 230–300 °C, and 300–500 °C, respectively. When Co/CS-C-IM was pretreated at 250 °C for 2 h (Fig. 16b), the TPR pattern showed that the first peak had disappeared and two reduction peaks at 276 °C, and between 300 and 600 °C were found. On pretreatment of Co/CS-C-IM at 350 °C for 2 h (Fig. 16c), the peak at 276 °C disappeared. According to the Co/N-CS study [14], the first peak is attributed to the reduction of Co_3O_4 to CoO. The second reduction peak is attributed to the reduction of CoO to Co^0. Compared to the TPR profile of the CS support (Fig. 16f), the third reduction peak at 477 °C for Co/CS-IM is attributed to the catalytic decomposition of the support. For CoA/CS-C-IM (Fig. 16d), three reduction peaks are also found in the TPR profile. The first reduction peak is at 314 °C, and the second reduction peak was centered at 363 °C. The third reduction peak is at 540 °C. It is noted that the TPR profile of Co/CS-DP shows only one reduction peak, located at 382 °C. In comparison with Co/CS-C-IM and CoA/CS-C-IM, the TPR profile of the cobalt catalyst supported on CSs by the deposition precipitation method did not show the reduction of Co_3O_4 to CoO, similar to that of Co/CNT-DP. This suggests that the CoO is also the main cobalt phase for the Co/CS-DP catalyst.

3.2. Fischer–Tropsch synthesis

Fischer–Tropsch synthesis performance of the Co/CNT and Co/CS catalysts was investigated in a fixed-bed micro-reactor at 225 °C and 0.8 MPa. It is believed that the active site for the cobalt catalysts in Fischer–Tropsch synthesis is metallic cobalt. Thus, a reduction step is indispensable in activating the catalysts. The autoreduction of Co/CS catalysts has been explored in a previous study [14], while the FTS performance of the autoreduced cobalt catalysts supported on CNTs, reported here, permits a comparison of the behavior of the two types of catalysts. The influence of the cobalt particle size on the activity, TOF, and C_{5+} selectivity for the Co/CNT and Co/CS catalyst has been compared.

3.2.1. Autoreduction of cobalt catalysts

As discussed above, cobalt oxide supported on both carbon nanotubes and carbon spheres can be reduced by the carbon supports. A previous study has reported on the autoreduction of Co/CS and the relative FTS performances of the catalysts [14]. In the present study, data on the FTS activity of cobalt supported on CNTs pretreated in H_2 and N_2 are given. The Fischer–Tropsch synthesis of the as-prepared Co/CNT-IM catalyst was investigated in a fixed-bed micro-reactor (Table 2) after pretreatment in both high-purity H_2 and high-purity N_2 at different temperatures (300, 400, and 480 °C). It should be mentioned firstly that the Co/CNT-IM catalyst

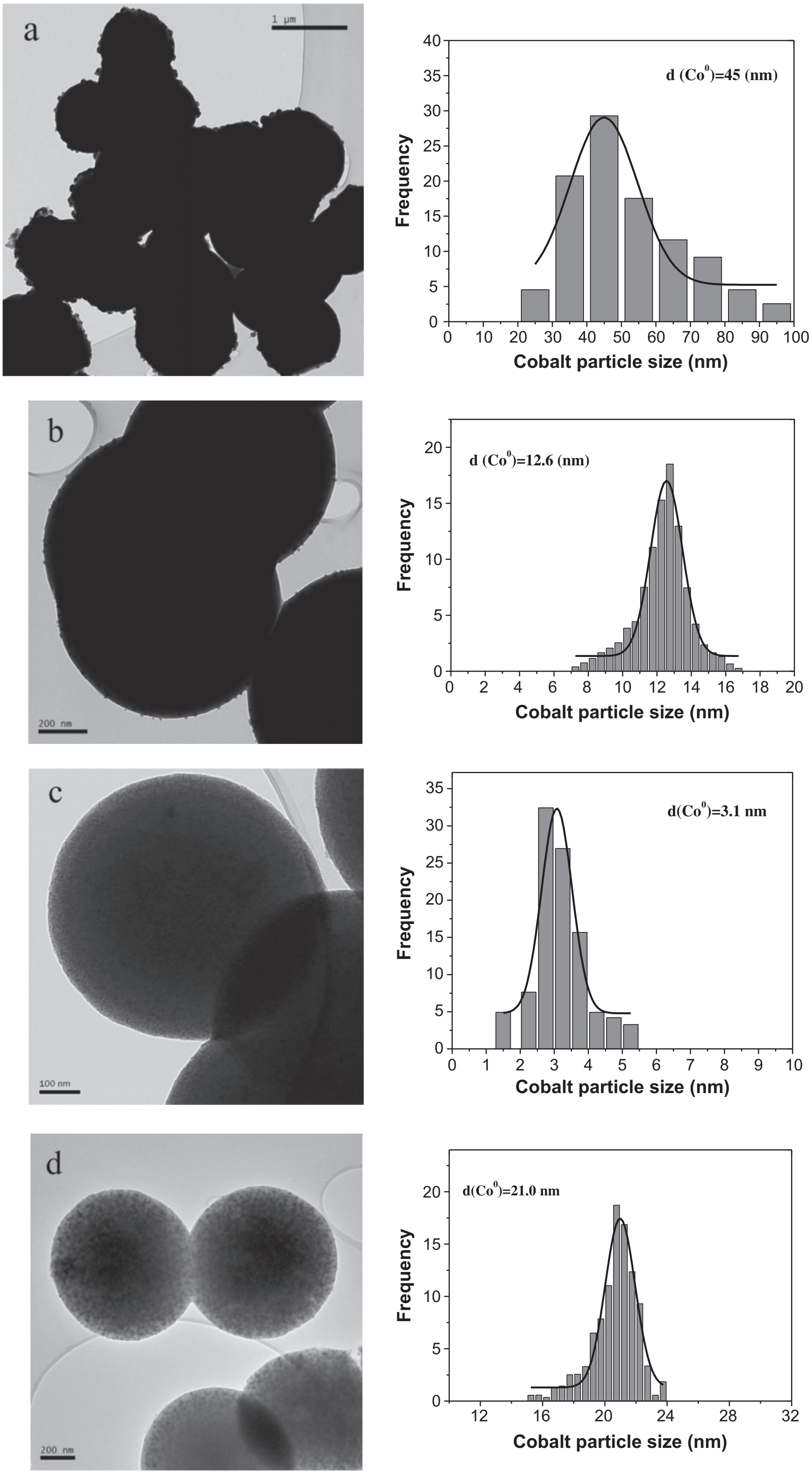

Fig. 12. Typical TEM images and cobalt particle size histograms of passivated Co/CS: (a) Co/CS-A-DP after reduction in H_2 at 400 °C for 20 h ($d(Co^0)$ = 45 nm); (b) Co/CS-B-DP after reduction in H_2 at 400 °C for 20 h ($d(Co^0)$ = 12.6 nm); (c) Co/CS-C-DP after reduction in H_2 at 400 °C for 20 h ($d(Co^0)$ = 3.1 nm); (d) Co/CS-B-DP after reduction in 5%H_2/Ar at 450 °C for 20 h ($d(Co^0)$ = 21 nm).

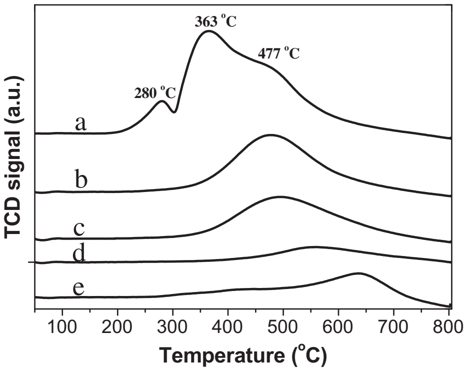

Fig. 13. TPR profiles for Co/CNT-IM catalyst and purified CNTs using different pretreatment temperatures in a flow of high-purity Ar for 2 h: (a) 250 °C; (b) 450 °C; (c) 550 °C; (d) 600 °C; (e) purified CNTs pretreated at Ar at 250 °C for 2 h.

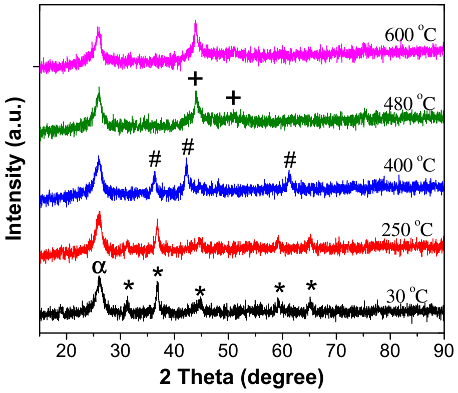

Fig. 14. In situ X-ray diffraction patterns of Co/CNT-IM catalyst with a function of temperature in N_2, α: carbon nanotubes, ∗: Co_3O_4, #: CoO, +: Co^0.

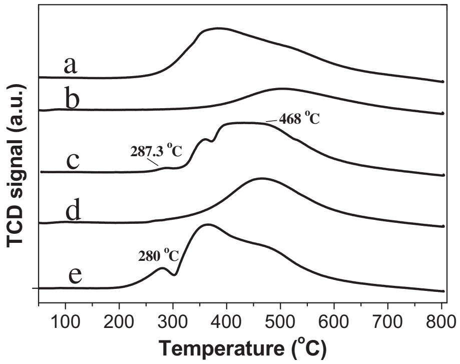

Fig. 15. TPR profiles for different Co/CNT catalysts pretreated in Ar: (a) Co/CNT-DP pretreated at 250 °C for 2 h; (b) Co/CNT-DP pretreated at 550 °C for 2 h; (c) CoA/CNT-IM pretreated at 250 °C for 2 h; (d) CoA/CNT-IM pretreated at 400 °C for 2 h; (e) Co/CNT-IM pretreated at 250 °C for 2 h.

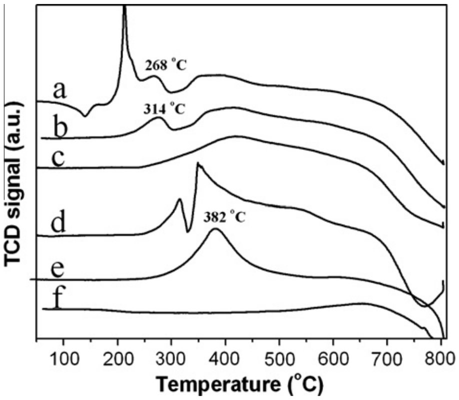

Fig. 16. TPR profiles for CSs and different Co/CS catalysts after different pretreatment temperatures in a flow of high-purity Ar for 2 h: (a) Co/CS-C-IM pretreated at 120 °C for 2 h; (b) Co/CS-C-IM pretreated at 250 °C for 2 h; (c) Co/CS-C-IM pretreated at 350 °C for 2 h; (d) CoA/CS-C-IM pretreated at 250 °C for 2 h; (e) Co/CS-C-DP pretreated at 250 °C for 2 h; (f) CSs pretreated at 250 °C.

pretreated under both atmospheres showed a good stability in the FTS reaction (Fig. S6). As can be seen, the data for the catalyst pretreated in H_2 revealed that the CO conversion of the catalyst increased when the pretreatment temperature was increased from 300 to 400 °C, while it decreased sharply when the temperature was increased to 480 °C. A TEM image (Fig. S7) of the spent Co/CNT-IM catalyst (i.e., after 200 h of FTS reaction) that had been pretreated with H_2 at 480 °C showed that big metallic cobalt particles (>50 nm) had formed on the surface of the support, while the catalysts pretreated with H_2 at both 300 and 400 °C showed well-defined smaller cobalt particles (Fig. 4 and Fig. S2a). It is noted that the big cobalt particles are formed during the H_2 reduction process prior to the FTS process for the passivated Co/CNT-IM catalyst pretreated in H_2 at 480 °C (Figs. S2 and S7). The big cobalt particles formed are due to reduction-induced sintering. Thus, the high CO activity for the catalysts treated under H_2 can be attributed to the small cobalt particles and high cobalt dispersion. When the Co/CNT-IM was pretreated in N_2, it was observed that the activity of the catalyst increased with the increase in pretreatment temperature from 400 to 480 °C. As demonstrated above, cobalt oxide can be reduced by the CNT support and the higher CO conversion should be attributed to the higher degree of catalyst reduction, resulting from the higher pretreatment temperature in N_2. It is also proposed, similar to studies with Co/CS [14], that the autoreduced catalyst resulted in the Co particles being “trapped” in cavities produced by the removal of surface carbon that was in contact with the cobalt oxide species prior to reduction (Fig. S8). This point can also be evidenced by the in situ XRD result which showed that the peak intensity (20–30°) of CNTs became weak and the peak became narrower after an increase in pretreatment temperature (Fig. S9).

The olefin/paraffin ratios in the FTS products are illustrated in Fig. S10. For the Co/CNT-IM catalyst pretreated in H_2 at 400 °C, a low olefin-to-paraffin ratio was observed. For the Co/CNT-IM catalyst pretreated in H_2 at 480 °C, a high olefin/paraffin ratio was present. The Co/CNT-IM catalysts pretreated in N_2 at 400 and 480 °C show comparable olefin/paraffin ratios. This correlates with the CO conversion data.

3.2.2. The effect of cobalt precursor, preparation methods, and cobalt particle size on the FTS performance

The FTS data for Co/CNT-IM pretreated under both H_2 and Ar at different temperatures indicated that pretreatment under H_2 at 400 °C gave the highest CO conversion. Thus, this pretreatment condition was chosen to investigate the FTS activity of the Co/CNT and Co/CS catalysts prepared using different methods and different cobalt precursors. The FTS performance of Co/CNT and Co/CS catalysts pre-reduced in H_2 at 400 °C is shown in Table 3. It is noted that the cobalt catalyst prepared from cobalt nitrate showed slightly higher CO conversion than the cobalt catalyst prepared from cobalt acetate.

The average cobalt particle size of Co/CNT and Co/CS catalysts studied is summarized in Table 4. The cobalt time yield (mol CO g^{-1} Co s^{-1}) was calculated and plotted as average cobalt

Table 2
Fischer–Tropsch synthesis performances of Co/CNT catalyst pretreated in high-purity H_2 and high-purity N_2 for 20 h.[a]

Sample	Pretreatment	CO conversion (%)	Product selectivity (mol%)				
			CH_4	C_2	C_3	C_4	C_{5+}
Co/CNT-IM	H_2 at 300 °C	12.5	11.1	0.5	1.3	1.4	85.8
	H_2 at 400 °C	25.9	30.6	1.4	2.9	3.1	62.1
	H_2 at 480 °C	3.7	2.9	0.2	0.5	0.5	95.9
	N_2 at 400 °C	3.4	3.5	0.1	0.3	0.3	95.8
	N_2 at 480 °C	13.3	8.9	0.6	1.7	1.8	87.0

[a] Reaction conditions: 225 °C, 0.8 MPa, $CO/H_2 = 1:2$, GHSV = 3840 h^{-1}, FTS data were collected at steady state (200 h).

Table 3
Fischer–Tropsch synthesis performances of Co/CNT and Co/CS catalysts pre-reduced in high-purity H_2 at 400 °C for 20 h.[a]

Sample	Cobalt loading (wt.%)	CO conversion (%)	Product selectivity (mol%)				
			CH_4	C_2	C_3	C_4	C_{5+}
Co/CNT-IM	13.23	25.9	30.6	1.4	2.9	3.1	62.1
CoA/CNT-IM	12.74	22.6	28.3	1.3	3.2	3.5	63.8
Co/CNT-DP	4.31	9.9	23.5	0.9	1.8	1.7	72.1
Co/CS-A-DP	0.98	1.8	2.4	0.1	0.2	0.4	97.0
Co/CS-B-DP	1.12	2.5	3.1	0.1	0.3	0.2	96.2
Co/CS-C-DP	1.47	3.7	4.0	0.2	0.5	0.5	94.8
CoA/CS-C-IM	5.11	2.4	0.7	0.1	0.2	0.2	98.8
Co/CS-C-IM	5.21	2.6	0.6	0.1	0.1	0.1	99.1

[a] Reaction conditions: 225 °C, 0.8 MPa, $CO/H_2 = 1:2$, GHSV = 3840 h^{-1}, FTS data were collected at steady state (200 h).

Table 4
Cobalt particle sizes and Fischer–Tropsch synthesis selectivities of Co/CNT and Co/CS catalysts at 4% CO conversion.[a]

Sample	Cobalt particle size (nm)		Product selectivity (mol%)				
	TEM (Co^0)	H_2-chemisorption (Co^0)[b]	CH_4	C_2	C_3	C_4	C_{5+}
Co/CNT-IM	3.9	4.5	4.1	0.3	0.4	0.3	94.9
Co/CNT-IM[c]	6.4	7.1	3.4	0.2	0.4	0.4	95.6
Co/CNT-IM[d]	12.4	14.3	3.5	0.1	0.3	0.3	95.8
CoA/CNT-IM	4.4	5.6	3.9	0.1	0.2	0.2	95.6
CoA/CNT-IM[e]	16.6	19.0	3.0	0.2	0.2	0.1	96.5
Co/CNT-DP	3.0	4.8	6.0	0.3	0.6	0.5	92.6
Co/CS-A-DP	45	62	1.9	0.1	0.2	0.1	97.7
Co/CS-B-DP	12.6	14.7	2.8	0.2	0.3	0.2	96.5
Co/CS-B-DP[f]	21	28.3	2.7	0.3	0.3	0.3	96.4
Co/CS-C-DP	3.1	4.8	4.0	0.2	0.5	0.5	94.8
Co/CS-C-IM	14.2	16.3	1.5	0.1	0.1	0.1	98.2

[a] Reaction conditions: 225 °C; 0.8 MPa; $CO/H_2 = 1:2$; FTS data were collected at steady state (200 h); catalyst was pre-reduced in high-purity H_2 at 400 °C for 20 h unless noted.
[b] Co particle size was obtained assuming hemispherical crystallites.
[c] Catalyst was pre-reduced in high-purity H_2 at 300 °C for 20 h.
[d] Catalyst was pretreated in high-purity N_2 at 480 °C for 20 h.
[e] Catalyst was pre-reduced in 5%H_2/Ar at 450 °C for 20 h.
[f] Catalyst was pre-reduced in 5%H_2/Ar at 450 °C for 20 h.

particle size for all the cobalt catalysts. As shown in Fig. 17a, a clear relationship between the cobalt time yield and cobalt particle size is observed such that smaller cobalt particles result in a higher cobalt time yield. A similar trend has been reported in a previous study for two Co/SiO_2 catalysts with different particle sizes [32]. Bezemer et al. however observed a volcano-like curve for Co/CNF catalysts when the cobalt time yield was plotted as a function of the cobalt particle size [11]. A possible explanation for the difference is that the aggregation of the Co^0 crystallites occurred during their FTS study and that the small cobalt particles aggregated more significantly than the large cobalt particles, leading to the decrease in cobalt time yield for the catalyst with small cobalt particles [32]. This did not occur in the present study.

The turnover frequency (TOF) of these cobalt catalysts based on H_2 chemisorption has also been calculated and plotted against cobalt particle sizes (Fig. 17b). As can be seen, the TOF is constant for cobalt particles above 10 nm but decreased sharply for the cobalt catalysts with smaller cobalt particles. Indeed, the impact of cobalt particle size on turnover frequency of FTS has been investigated by others [11,33–37]. Iglesia et al. [33] found that the intrinsic site reaction rate does not depend on the Co particle size in the range of ca. 10–200 nm. Bezemer et al. [11] have suggested a non-classical structure sensitivity for Co catalysts supported on inert carbon nanofibers (Co/CNF). The TOF increases for particles that are smaller than 6–8 nm continuously and remains invariant for larger particles. This behavior differs from classical structure sensitivity which is related to the metal surface crystallographic anisotropy and becomes apparent only when the particle size is reduced typically below 3–4 nm [38]. More recently, den Breejen et al. reported that cobalt particles of 4.7 ± 0.2 nm are the most active in

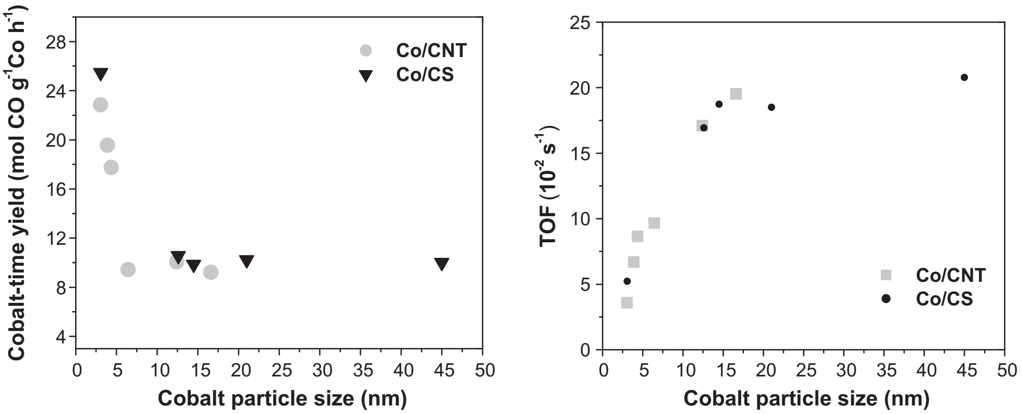

Fig. 17. The influence of cobalt particle size on the activity and turnover frequency of both Co/CNT and Co/CS (Reaction conditions: $CO/H_2 = 1:2$, 225 °C, 0.8 MPa, GHSV = 3840 h^{-1}).

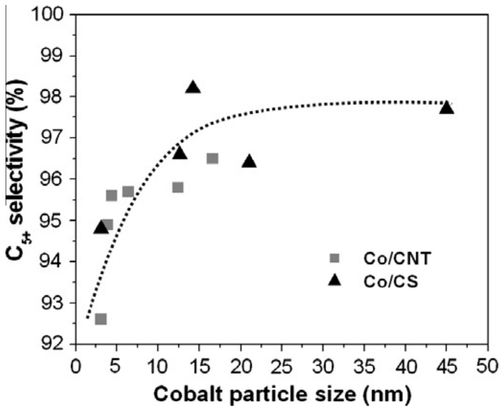

Fig. 18. The influence of cobalt particle size on C_{5+} selectivity of Co/CNT and Co/CS at 4% CO conversion by changing space velocity (Reaction conditions: $CO/H_2 = 1:2$, 225 °C, 0.8 MPa). Black dotted line is the trendline for all catalysts.

the FT reaction (1 bar, 220 °C) [39]. Prieto and coworkers [37] studied the effect of cobalt particle size effect on the TOF of FTS employing Co/ITQ-2 as model catalysts, and a similar relationship between cobalt particle size and TOF was obtained.

The effect of cobalt particle size on the hydrocarbon selectivity of FTS was also investigated. It has been reported that C_{5+} selectivity can be affected by the amount of water produced at different CO conversions. To overcome this, the present study compared the effect of cobalt particle size on the C_{5+} at a low CO conversion (4.0%) to minimize the effect of water. The cobalt particle size and C_{5+} selectivity are displayed in Table 4 and plotted in Fig. 18. As can be seen, a positive relationship was observed between cobalt particle size and C_{5+} selectivity *for both Co/CNT and Co/CS catalysts*. The change in C_{5+} selectivity with particle size seems reasonable because it is believed that bridge-type adsorbed CO is more easily formed on large Co particles [28]. The bridge-type CO is much more active than linear-type CO because it has a weaker C–O bond and thus can be more easily dissociated to carbon and oxygen. An increased CH_x ($1 \leqslant x \leqslant 3$) concentration on a large Co particle can enhance the chain growth and thus increase the C_{5+} selectivity. Compared to the C_{5+} selectivity obtained for Co/CNT, the Co/CS exhibited a slightly higher C_{5+} selectivity for a similar sized particle. For our CNT catalysts, active sites are situated predominantly not exclusively outside the tube. Thus, a proportion of light hydrocarbons obtained from the Co/CNT catalyst may be due to the greater rate of diffusion of hydrogen compared with that of carbon monoxide within the tube. The gas reaching the catalyst inside the tube is thus richer in hydrogen than in the synthesis gas [40]. For Co catalysts supported on non-porous carbon spheres, *all cobalt particles are dispersed on the outer surface of the support*. The hydrogen concentration around the active metal cobalt is the same as that in the reactor. Thus, less light hydrocarbons will be produced for Co/CS during FTS, as observed.

A previous study on Co/γ-Al_2O_3 catalysts reported that the product selectivity of FTS can be affected by cobalt particle size [41]. A positive correlation between cobalt particle size (above 10 nm) and C_{5+} selectivity was found by investigating the influence of cobalt particle size in the range 3–18 nm. The authors reported that the maximum C_{5+} selectivity was located at 7–8 nm [42] and that the C_{5+} selectivity was not only related to the cobalt particle size but also to the choice of support.

4. Conclusions

Carbon nanotubes and carbon spheres were prepared by chemical vapor deposition. Co/CNT and Co/CS catalysts with cobalt particle size ranging from 3 to 45 nm were prepared by different methods using different cobalt precursors. It was found that the cobalt catalysts supported on CNTs and CSs can be autoreduced by the supports in an inert atmosphere at ca. 480 °C. In both cases, the cobalt catalysts that are autoreduced in an inert atmosphere show better Fischer–Tropsch performance than those catalysts reduced in H_2 at the same temperature. This lower activity of the cobalt catalysts reduced in H_2 when the temperature is higher than 400 °C is due to enhanced sintering. It is noted that the FT activity using H_2 reduction is better at $T = 400$ °C but reduction under N_2 is better at $T = 480$ °C.

Cobalt particle size has been found to have an impact on the cobalt time yield, turnover frequency (TOF), and C_{5+} selectivity for both Co/CNT and Co/CS catalysts. A direct relation between the cobalt time yield and cobalt particle size is observed such that a smaller cobalt particle results in higher cobalt time yield. The TOF value for both Co/CNT and Co/CS was constant for cobalt particles above 10 nm and decreased sharply for the cobalt catalysts with smaller cobalt particles. Finally, a positive relationship was observed between cobalt particle size and C_{5+} selectivity for both Co/CNT and Co/CS catalysts.

It is clear that the Co/CS and Co/CNT catalysts behave similarly and any differences relate to the surface area and/or dispersion effects associated with the two different carbon supports. Since CSs are easier to prepare than CNTs and contain no metal impurities, they provide better model supports to explore cobalt–carbon interactions than CNTs. The disadvantage of using our CSs relates to their low surface areas. Current studies are centered on generating CSs with larger surface areas to overcome this limitation.

Acknowledgments

This work was supported financially by the DST/NRF Centre of Excellence in Strong Materials, a SPARC fellowship (HX) and the University of the Witwatersrand. We thank M.K. Rayner and Prof. D.G. Billing for XRD measurements.

Appendix A. Supplementary material

Supplementary data associated with this article can be found, in the online version, at doi:10.1016/j.jcat.2010.11.010.

References

[1] M.S. Luo, H. Hamdeh, B.H. Davis, Catal. Today 140 (2009) 127.
[2] A. Martínez, G. Prieto, J. Rollán, J. Catal. 263 (2009) 292.
[3] W. Chen, Z.L. Fan, X.L. Pan, X.H. Bao, J. Am. Chem. Soc. 130 (2008) 9414.
[4] A.K. Dalai, B.H. Davis, Appl. Catal. A 348 (2008) 1.
[5] E. de Smit, I. Swart, J.F. Creemer, G.H. Hoveling, M.K. Gilles, T. Tyliszczak, P.J. Kooyman, H.W. Zandbergen, C. Morin, B.M. Weckhuysen, F.M.F. de Groot, Nature 456 (2008) 222.
[6] T. Mochizuki, T. Hara, N. Koizumi, M. Yamada, Appl. Catal. A 317 (2007) 97.
[7] A.Y. Khodakov, W. Chu, P. Fongarland, Chem. Rev. 107 (2007) 1692.
[8] G. Jacobs, J.A. Chaney, P.M. Patterson, T.K. Das, B.H. Davis, Appl. Catal. A 264 (2004) 203.
[9] B. Jongsomjit, J. Panpranot, J.G. Goodwin Jr, J. Catal. 215 (2003) 66.
[10] J.L. Li, N.J. Coville, Appl. Catal. A 181 (1999) 201.
[11] G.L. Bezemer, J.H. Bitter, H.P.C.E. Kuipers, H. Oosterbeek, J.E. Holewijn, X. Xu, F. Kapteijn, A.J. van Dillen, K.P. de Jong, J. Am. Chem. Soc. 128 (2006) 3956.
[12] J.P. den Breejen, P.B. Radstake, G.L. Bezemer, J.H. Bitter, V. Frøseth, A. Holmen, K.P. de Jong, J. Am. Chem. Soc. 131 (2009) 7197.
[13] J.C. Kang, S.L. Zhang, Q.H. Zhang, Y. Wang, Angew. Chem. Int. Ed. 48 (2009) 2565.
[14] H.F. Xiong, M. Moyo, M.K. Rayner, L.L. Jewell, D.G. Billing, N.J. Coville, ChemCatChem 2 (2010) 514.
[15] P. Serp, E. Castillejos, ChemCatChem 2 (2010) 41.
[16] M.C. Bahome, L.L. Jewell, D. Hildebrandt, D. Glasser, N.J. Coville, Appl. Catal. A 287 (2005) 60.
[17] L. Guczi, G. Stefler, O. Geszti, Zs. Koppány, Z. Kónya, E. Molnár, M. Urbán, I. Kiricsi, J. Catal. 244 (2006) 24.
[18] R.M. Malek Abbaslou, A. Tavassoli, J. Soltan, A.K. Dalai, Appl. Catal. A 367 (2009) 47.
[19] M. Trépanier, A. Tavasoli, A.K. Dalai, N. Abatzoglou, Appl. Catal. A 353 (2009) 193.
[20] H. Zhang, C. Lancelot, W. Chu, J.P. Hong, A.Y. Khodakov, P.A. Chernavskii, J. Zheng, D.G. Tong, J. Mater. Chem. 19 (2009) 9241.
[21] Z.L. Wang, Z.C. Kang, J. Phys. Chem. 100 (1996) 17725.
[22] Z.C. Kang, Z.L. Wang, J. Mol. Catal. A: Chem. 118 (1997) 215.
[23] H.F. Xiong, M. Moyo, M.A.M. Motchelaho, L.L. Jewell, N.J. Coville, Appl. Catal. A 388 (2010) 168.
[24] A. Nieto-Márquez, D. Toledano, J.C. Lazo, A. Romero, J.L. Valverde, Appl. Catal. A 373 (2010) 192.
[25] A. Nieto-Márquez, D. Toledano, P. Sánchez, A. Romero, J.L. Valverde, J. Catal. 269 (2010) 242.
[26] J.J. Delgado, X. Chen, J.P. Tessonnier, M.E. Schuster, E. Del Rio, R. Schlögl, D.S. Su, Catal. Today 150 (2010) 49.
[27] S.D. Mhlanga, K.C. Mondal, R. Carter, M.J. Witcomb, N.J. Coville, S. Afr. J. Chem. 62 (2009) 67.
[28] A. Moen, D.G. Nicholson, Chem. Mater. 9 (1997) 1241.
[29] G.L. Bezemer, P.B. Radstake, V. Koot, A.J. van Dillen, J.W. Geus, K.P. de Jong, J. Catal. 237 (2006) 291.
[30] H.F. Xiong, Y.H. Zhang, K.Y. Liew, J.L. Li, J. Mol. Catal. A: Chem. 295 (2008) 68.
[31] R.C. Haddon, Science 261 (1993) 1545.
[32] G.Z. Bian, N. Fujishita, T. Mochizuki, W.S. Ning, M. Yamada, Appl. Catal. A 252 (2003) 251.
[33] E. Iglesia, S.L. Soled, R.A. Fiato, J. Catal. 137 (1992) 212.
[34] S.W. Ho, M. Houlalla, D.M. Hercules, J. Phys. Chem. 94 (1990) 6396.
[35] A. Barbier, A. Tuel, I. Arcon, A. Kodre, G.A. Martin, J. Catal. 200 (2001) 106.
[36] T. Herranz, X.Y. Deng, A. Cabot, J.G. Guo, M. Salmeron, J. Phys. Chem. B 113 (2009) 10721.
[37] G. Prieto, A. Martínez, P. Concepción, R. Moreno-Tost, J. Catal. 266 (2009) 129.
[38] M. Boudart, Chem. Rev. 95 (1995) 661.
[39] J.P. den Breejen, J.R.A. Sietsma, H. Friedrich, J.H. Bitter, K.P. de Jong, J. Catal. 270 (2010) 146.
[40] R.B. Anderson, W.K. Hall, A. Krieg, B. Seligman, J. Am. Chem. Soc. 71 (1949) 183.
[41] Ø. Borg, S. Eri, E.A. Blekkan, S. Storsæter, H. Wigum, E. Rytter, A. Holmen, J. Catal. 248 (2007) 89.
[42] Ø. Borg, P.D.C. Dietzel, A.I. Spjelkavik, E.Z. Tveten, J.C. Walmsley, S. Diplas, S. Eri, A. Holmen, E. Rytter, J. Catal. 259 (2008) 161.